Results in Physics 11 (2018) 591–598

Contents lists available at ScienceDirect

Results in Physics

journal homepage: www.elsevier.com/locate/rinp

# Cohesive zone modeling of hydrogen-induced delayed intergranular fracture in high strength steels

Weijie Wu[a,b], Yanfei Wang[a,*], Ping Tao[b], Xinfeng Li[c], Jianming Gong[b]

[a] School of Chemical Engineering & Technology, China University of Mining and Technology, Xuzhou 221116, China
[b] School of Mechanical and Power Engineering, Nanjing Tech University, Nanjing 211800, China
[c] School of Mechanical and Materials Engineering, Washington State University, Pullman, WA 99164, USA

ARTICLE INFO

*Keywords:*
Hydrogen-induced delayed fracture
Hydrogen traps
Thermodynamic decohesion theory
Cohesive zone modeling

ABSTRACT

A sequentially coupled hydrogen diffusion-cohesive zone modeling approach was applied to the simulation of hydrogen-induced delayed intergranular (IG) fracture in high-strength low-alloy steels. The effects of multiple hydrogen trap sites and mechanical deformation on the diffusion and cohesive strength of grain boundaries (GB) were taken account, in order to reveal that the hydrogen trapped at GB play a dominant role in the degradation processes of hydrogen of high-strength low-alloy steels, which leads to the IG fracture. The approach was implemented by Abaqus software in the form of a two-steps procedure including the coupled elastoplastic-transient hydrogen diffusion analysis and cohesive stress analysis. To validate the approach, the constant load tests of hydrogen pre-charged AISI 4135 high-strength low-alloy steel notched bars in literature were analyzed. Good agreement is observed between the simulation and experimental data of time to failure. The results confirm that hydrogen-induced IG fracture of high strength low-alloy steels can be related to the hydrogen concentration trapped at GB. The critical hydrogen concentration at GB for crack initiation is independent of the initial hydrogen concentration but depends strongly on the local stress level and stress triaxiality. The critical hydrogen concentration linearly decreases with increasing normalized peak maximal principal stress normalized by the critical cohesive strength in absence of hydrogen.

## Introduction

In the industries of aerospace, auto and energy, the applications of high-strength low-alloy steels for components enable higher operation parameters and lighter and cheaper products [1]. However, a large number of studies have shown that the high-strength steels are very susceptible to hydrogen-induced delayed fracture (HIDF) [2,3]. Typically, there is an incubation time for hydrogen diffusing to the highly stressed zone before fracture occurs. During this period, little deformation and no cracks can be detected [2]. Thus, the fracture might happen unexpectedly. Akin to the other degradation phenomena caused by hydrogen, the involved processes of HIDF include the hydrogen introduction due to environmental exposure or manufacturing processes such as welding and electroplating, hydrogen transport and accumulation to potential crack initiation sites, and micro-scale hydrogen degradation mechanism [1,4]. Unfortunately, the hydrogen degradation mechanism remains contentious. Among the proposed mechanisms, hydrogen-enhanced decohesion (HEDE) [5–7] and hydrogen-enhanced localized plasticity (HELP) are the most accepted [8,9]. The core of HEDE mechanism is that hydrogen can weaken the lattice or interface cohesive strength hence assists the separations of cleavage planes or grain boundaries (GB) under a lower stress [5–7]. The resulting fracture mode is thus transgranular cleavage/quasi-cleavage (QC) and intergranular (IG), respectively. While HELP mechanism argues that hydrogen can promote dislocation motion and hence cause localized deformation, consequently leading to reduced macroscopic ductility of metals [8,9]. Since HELP is associated with dislocation emission from the plastic zone ahead of a crack tip, the resulting fracture surfaces may characteristically ductile, for example, still exhibiting microvoid coalescence (MVC) fracture mode (But compared with the hydrogen-free materials, the dimples may be smaller and shallower) [10,11].

More recently, it is further considered that the two mechanisms may act simultaneously in many cases and the feature of a given material-hydrogen system influences the dominating mechanism. For instance, Novak et al. [12] established a statistical, physical-based, micro-mechanical model of hydrogen-induced IG fracture in steels to advocate the synergistic action of HELP and HEDE. Djukic et al. [13–16] detected the simultaneous action of HELP and HEDE based on a special approach

* Corresponding author.
*E-mail address:* wyf_hg@cumt.edu.cn (Y. Wang).

https://doi.org/10.1016/j.rinp.2018.10.001
Received 31 July 2018; Received in revised form 19 September 2018; Accepted 1 October 2018
Available online 06 October 2018

applied in subsequent post-mortem investigations of samples unevenly enriched with hydrogen and damaged during the actual operation of an industrial component, they confirmed that HELP + HEDE can be active depending on the local concentration of hydrogen in the investigated low carbon steel. Nagao et al. [17–20] revealed a mechanism that can be termed as hydrogen-enhanced-plasticity mediated decohesion, based on the transmission electron microscopy (TEM) analyses [17–20] of samples lifted from beneath fracture surfaces through focused ion beam machining. They argued that IG cracking takes place by dislocation pile-ups impinging on the prior austenite grain boundaries and "quasi-cleavage" is the case when dislocation pile-ups impinge on the block boundaries. These boundaries, whose cohesive strength has already been weakened by the presence of hydrogen, are debonded by the pile-up stresses [17–20]. It seems that HELP may inevitably play a role in various material-hydrogen systems, however, for the high-strength low-alloy steels examined here, such as the AISI 4xxx series steels, HEDE can still be regarded as the dominant mechanism, as on one hand these steels exhibit IG fracture mode after severe hydrogenation [1–3], and on the other hand many mechanical models and quantum-mechanical calculations based on HEDE provide good predictions of hydrogen-induced fracture [4,7,21,22].

It should be noted that, when hydrogen-related failure is discussed, there is often a concept of critical hydrogen concentration examined by different researchers for the transition of different phenomena. For instance, when reaching a critical hydrogen concentration, Lunarska et al. [23] revealed a change in the damage mechanism from the decohesion of GB to the formation of micro crevices at GB and phase boundaries. Capelle et al. [24] defined the term "critical hydrogen concentration" as the concentration level at the time of critical loss of local strength of the materials at the notch tip in the presence of hydrogen, and Djukic et al. [13–16] defines it as that causes critical drop in the impact strength of material and the sharp ductile–brittle fracture transition. However, in the fracture mechanics tests of high-strength low-alloy steels, it is generally believed that when the local hydrogen concentration at the highly stressed site ahead of a crack tip or notch root exceeds a critical value via stress-enhanced hydrogen accumulation, cracking initiation occurs [1,2,7]. In such cases, the critical hydrogen concentration represents the concentration level causing the formation of new surfaces. This supports the HEDE mechanism, as which assumes that, with increasing hydrogen concentration level, the cohesive strength of interfaces decreases gradually, till interface debonding occurs. Moreover, for the high strength steels, it seems that hydrogen trapped locally at GB play a more dominant role in the cohesive strength degradation of hydrogen [1,12,17–20], which leads to IG fracture after reaching the critical GB hydrogen concentration by weakening the cohesive strength of GB following the HEDE mechanism.

Cohesive zone modeling (CZM), which uses cohesive elements governed by a constitutive response defined by a traction-separation law (TSL) for conventional fracture simulation, has gained increasing attention in hydrogen-induced fracture as its capacity in representing the involved micro-processes combined with the benefit in saving manpower and cost. In the CZM simulation of hydrogen-induced fracture, hydrogen degradation effect can be implemented into the TSL by various approaches including the quantum-mechanical calculation [4], fitting the damage law [25] and classic decohesion theory of thermodynamics [26]. The simulation of hydrogen-induced fracture requires modeling the interacting processes of transient hydrogen diffusion, mechanical deformation and hydrogen degradation effects [27]. Serebrinsky et al. [4] presented a fully coupled CZM approach taking account of these interacting processes. Their approach reproduced the experimental trends of hydrogen-assisted crack initiation and growth with the dependence of applied stress intensity, hydrogen content, temperature and yield strength of material. Olden et al. [28] developed a three-steps sequential coupled CZM approach, i.e., stress analysis, diffusion analysis and cohesive analysis. Despite many modeling techniques, the effect of hydrogen trapping must be taken into account. As pointed out by the review of Jemblie et al. [27], the choice of hydrogen trapping parameters has a significant impact on the hydrogen distribution and resulting hydrogen-induced damage. Some papers [25,29] have implemented the effect of hydrogen trapped dislocations into the TSL, which reproduced the experimental data. However, few researches consider the effect of multiple trap sites on hydrogen diffusion. For the high strength steels, since it seems that hydrogen trapped at GB leads to the intergranular fracture after reaching the critical hydrogen concentration, the effect of multiple trap sites including both the dislocations and GB should be considered.

The objective of this paper is to develop a two-steps sequential coupled diffusion-CZM approach to model the HIDF of high-strength low-alloy steels. The effects of both multiple trap sites and mechanical deformation on the hydrogen transport were included in the approach. The hydrogen damage was implemented into the TSL based on the classic thermodynamic decohesion theory. To validate the approach, the constant load tests of notch bars of AISI 4135 steel performed by Wang et al. [2] were simulated by considering the trapping effect of both dislocations and GB. The simulation results were compared with the experimental data. To further investigate the effects of initial hydrogen concentration, notch radius and load level, parametric studies were also performed.

## Coupled diffusion-CZM approach

Hydrogen resides at normal interstitial lattice sites (NILS) or trap sites such as dislocations, GB and carbides [30]. The hydrogen concentration $C_L$ in NILS can be written as $C_L = \theta_L N_L$ where $\theta_L$ is the hydrogen occupancy of NILS, $N_L$ denotes the number of NILS. Similarly, the hydrogen concentration $C_{T,k}$ in the k type of trap sites can be expressed as $C_{T,k} = \theta_{T,k} N_{T,k}$ where $\theta_{T,k}$ denotes the occupancy of type k trap sites and $N_{T,k}$ is the corresponding trap site density. Oriani assumes local equilibrium between hydrogen at trap sites and NILS [31], thus we can write

$$\frac{\theta_{T,k}(1-\theta_L)}{\theta_L(1-\theta_{T,k})} = \exp\left(\frac{\Delta g^0_{T,k}}{RT}\right) = K_{T,k} \tag{1}$$

where $\Delta g^0_{T,k}$ is the binding energy of hydrogen with the type k trap sites and $K_{T,k}$ denotes the corresponding equilibrium constant. According to the conservation equation of diffusing material ($dC/dt = -\nabla J$, where $C = C_L + \sum_k C_{T,k}$ is the total hydrogen concentration, $t$ is the time and $J$ is the flux of hydrogen) and the extension of Fick's equation ($J = -D_L C_L/RT \cdot \nabla\mu$, where $D_L$ is the diffusion coefficient of hydrogen at NILS in the trap-free material, $\mu$ is the chemical potential, $R = 8.314$ J/(mol·K) is the gas constant, and $T$ is the temperature), which considers the chemical potential gradient of hydrogen at NILS ($\mu = \mu_0 + RT\ln C_L - V_H\sigma_h$, where $\mu_0$ is a fixed datum, $\sigma_h$ is the hydrostatic stress, and $V_H = 2.1$ cm$^3$/mol is the partial molar volume of hydrogen in steels) as the driven force for diffusion of hydrogen, we can write

$$\frac{d}{dt}\left(C_L + \sum_k C_{T,k}\right) = \nabla\cdot(D\nabla C_L) - \nabla\cdot\left(\frac{D_L V_H}{RT} C_L \nabla\sigma_h\right) \tag{2}$$

Based on Eq. (1), we can get

$$\frac{dC_{T,k}}{dt} = \theta_{T,k}\frac{dN_{T,k}}{dt} + \frac{N_{T,k}}{N_L}\frac{K_{T,k}}{(1+K_{T,k}\theta_L)^2}\frac{dC_L}{dt} \tag{3}$$

Hence, Eq. (2) becomes

$$\left(1 + \sum_k \frac{N_{T,k}}{N_L}\frac{K_{T,k}}{(1+K_{T,k}\theta_L)^2}\right)\frac{dC_L}{dt} + \sum_k \theta_{T,k}\frac{dN_{T,k}}{dt} = \nabla\cdot(D\nabla C_L) - \nabla\cdot\left(\frac{D_L V_H}{RT} C_L \nabla\sigma_h\right) \tag{4}$$

Quenched and tempered martensitic high-strength steels are

considered, which typically manifest a transition from dimple fracture for hydrogen-free specimens to intergranular fracture for hydrogen-charged specimens. As mentioned, the latter is believed to be associated with the hydrogen-induced decohesion of GB. Thus, two types of trap sites i.e. dislocation trap sites and GB trap sites are considered. The subscript k in Eq. (4) is replaced by "d" and "gb" to denote the dislocation trap sites and GB trap sites, respectively, and since the density of GB trap sites does not vary with deformation, i.e. $dN_{T,gb}/dt = 0$ (Note that, $dN_{T,d}/dt \neq 0$, because dislocation density increases with plastic deformation), Eq. (4) becomes

$$\left(1+\frac{N_{T,d}}{N_L}\frac{K_{T,d}}{(1+K_{T,d}\theta_L)^2}+\frac{N_{T,gb}}{N_L}\frac{K_{T,gb}}{(1+K_{T,gb}\theta_L)^2}\right)\frac{dC_L}{dt}+\theta_{T,d}\frac{dN_{T,d}}{dt} = \nabla\cdot(D\nabla C_L)-\nabla\cdot\left(\frac{D_L V_H}{RT}C_L\nabla\sigma_h\right) \tag{5}$$

where $N_{T,d}$ and $K_{T,d}$ are the dislocation trap densities and the corresponding equilibrium constant, and $N_{T,gb}$ and $K_{T,gb}$ are the GB trap densities and the corresponding equilibrium constant. Eq. (5) is the hydrogen diffusion model considering the combined effects of multiple trap sites (GB trap sites and dislocation trap sites) and mechanical deformation.

Hirth–Rice–Wang's theory of thermodynamic decohesion [32,33] is employed to describe the degradation effect of hydrogen on the separations of GB. The cohesive energy of GB is reduced by hydrogen as the following equation [26,33]

$$2\gamma_{gb}^{H} = 2\gamma_{gb}^{0}-(\Delta g_{T,gb}^{0}-\Delta g_{T,FS}^{0})\Gamma \tag{6}$$

where $2\gamma_{gb}^{H}$ denotes the cohesive energy of GB with hydrogen influence, $2\gamma_{gb}^{0}$ is the cohesive energy of hydrogen-free GB, $\Delta g_{T,gb}^{0}$ and $\Delta g_{T,FS}^{0}$ are the hydrogen binding energy of GB and free surfaces respectively, and $\Gamma$ is the hydrogen coverage of GB. With the consideration of a monolayer type of GB, the hydrogen coverage $\Gamma$ can be related to the hydrogen occupancy of GB by $\Gamma/\Gamma_{max} = \theta_{T,gb}$ where $\Gamma_{max}$ is the saturated hydrogen coverage of GB. Based on the relationship between the grain-boundary hydrogen coverage and cohesive energy and given a constant critical interfacial separation $\delta_c$ [4], the critical cohesive strength of GB $\sigma_c(\theta_{T,gb})$ due to hydrogen segregation can thus be calculated through the hydrogen occupancy $\theta_{T,gb}$ by

$$\frac{\sigma_c(\theta_{T,gb})}{\sigma_c(0)} = \frac{2\gamma_{gb}^{H}}{2\gamma_{gb}^{0}} = 1-\frac{\Gamma_{max}(\Delta g_{T,gb}^{0}-\Delta g_{T,FS}^{0})}{2\gamma_{gb}^{0}}\theta_{T,gb} \tag{7}$$

A modified linear decreasing cohesive law is chosen for the simulation of brittle intergranular fracture. The formulation is [34]

$$\sigma(\delta) = \begin{cases}\sigma_c\frac{\delta}{\delta_0}, & \delta < \delta_0\\ \sigma_c\left(\frac{\delta_c-\delta}{\delta_c-\delta_0}\right), & \delta_0 < \delta < \delta_c\end{cases} \tag{8}$$

where $\delta_0$ denotes the elastic separation. Fig. 1 shows schematically the variation of the shape of TSL with different hydrogen occupancy of GB.

In present study, we build a two-steps finite element procedure modified from the approach of Olden et al. [28,29] and based on the sequential coupling FE procedure of Jiang et al. [35–37] to simulate the hydrogen-induced intergranular fracture. The first step is coupled elastoplastic-transient hydrogen diffusion analysis to generate the hydrogen distribution for cohesive elements based on Eq. (5). This analysis is implemented in ABAQUS with several user defined subroutines, including USDFLD, UMAT and UMATHT, using the analogy between mass diffusion equation and heat transfer equation (the form of the two equations is identical), as noted by Díaz et al. [38] and Barrera et al. [39]. One can refer to [38,39] for details of the analogy and calculational procedure. The following step is cohesive stress analysis with the addition of hydrogen dependent TSL to the cohesive elements along crack path to simulate the hydrogen-induced fracture based on Eq. (8). The hydrogen concentration information needed for the cohesive stress analysis is given using a mean concentration of the nodes connected to the cohesive elements [28]. The loading time increases until the failure of a cohesive element is observed.

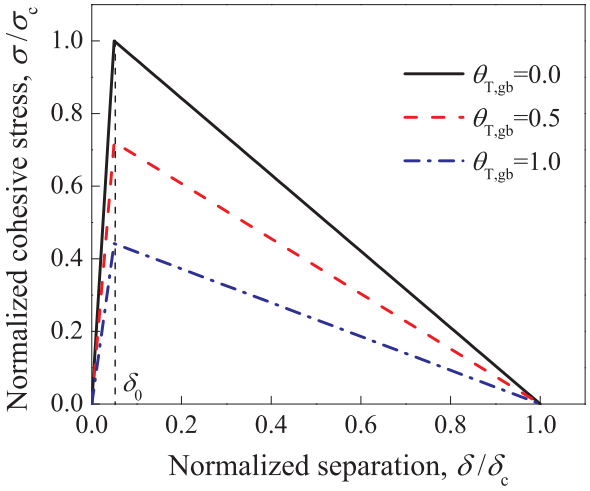


**Fig. 1.** Hydrogen dependent traction separation law.

## Numerical model

The constant load tests of notched bars of quenched and tempered martensitic AISI 4135 steel performed by Wang et al. [2] are simulated, in order to validate the proposed calculation approach above for hydrogen-induced fracture. The tested materials were prepared from AISI 4135 steel with two strength grades, i.e. B13 (tensile strength $\sigma_B$ = 1320 MPa) and B15 ($\sigma_B$ = 1450 MPa). Fig. 2 shows a schematic of the modelled domain. The specimen geometry is the same as that of the tested specimens in [2]. Due to symmetry, a quarter of specimen was modelled. The model was assigned with four-node coupled displacement-temperature axisymmetric solid elements in the coupled elasto-plastic-transient diffusion analysis. The cohesive elements were inserted at the mid-section. The size of the cohesive elements is set as 0.5 μm, as Olden et al. have reported that the element size should be smaller than 5 μm (or $\delta_c/d > 0.04$, $d$ is the mesh size of cohesive zone) to sufficiently resolve the local cohesive stress field of cohesive zone [28]. To overcome the convergence problem, a value of viscosity of $1 \times 10^{-4}$ was used in the ABAQUS program, as Yu et al. [40] have reported that when the value of viscosity is small enough, e.g. $1 \times 10^{-4}$, the results can give perfect prediction of the fracture. A constant load $\sigma_{app}$ is applied on the ends of specimen. The outer boundaries of the modelled domain were prescribed to have zero hydrogen flux as the specimen surfaces had been electroplated with Cd after hydrogen-charging in [2].

The initial hydrogen content throughout the model was obtained by calculating from the experimental data of diffusible hydrogen content determined by thermal desorption spectroscopy (TDS). The diffusible hydrogen is the hydrogen desorbed at the first peak of the TDS spectrum, which is the sum of hydrogen in the NILS and reversible traps [2,3]. Since carbide traps are irreversible due to their high binding energy with hydrogen [41,42], dislocations and GBs were considered as the main reversible traps. Hence, based on Oriani's equilibrium assumption, the initial hydrogen concentration at various sites, i.e. at NILS $C_{L0}$, dislocation trap sites $C_{T,d0}$ and GB trap sites $C_{T,gb0}$, can be determined by the diffusible hydrogen content $C_D$ by Eq. (1) as

$$\begin{cases} C_D = C_{L0} + C_{T,d0} + C_{T,gb0} \\ C_{T,d0} = \frac{N_{T,d}K_{T,d}C_{L0}}{K_{T,d}C_{L0}+N_L} \\ C_{T,gb0} = \frac{N_{T,gb}K_{T,gb}C_{L0}}{K_{T,gb}C_{L0}+N_L} \end{cases} \tag{9}$$

Inserting $C_D$ data from [2,3] into Eq. (7), the initial hydrogen

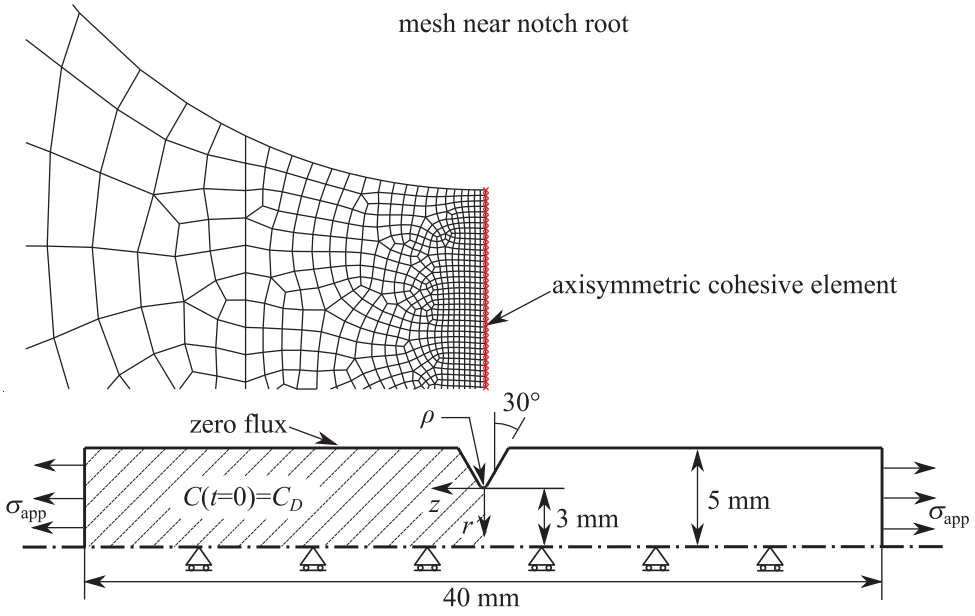


**Fig. 2.** Finite element model of the notched specimens.

concentrations at NILS, dislocation trap sites and GB trap sites were obtained and then were assigned to the modelled domain.

The material properties for diffusion analysis are collected in Table 1. The diffusion coefficients $D_L$ of the B13 and B15 free of dislocation and GB trap sites were assigned the value of $2.5 \times 10^{-5}$ and $4.0 \times 10^{-5}$ mm$^2$/s, respectively, according to [2]. The increase of dislocation trap sites $N_{T,d}$ due to plastic deformation is considered, which is related to dislocation density $\rho_d$ by $N_{T,d} = \sqrt{2}\rho_d/a$ [43], where $a$ is the lattice parameter. Since there is no experimental measurement of the variation of $\rho_d$ with plastic deformation for AISI 4135 steel, we estimate the dislocation density at a given plastic deformation level by Taylor-like equation, i.e., $\sigma_e = \sigma_r + 2\alpha Gb\sqrt{\rho_d}$ [44,45], where $\sigma_e$ is the resulting Mises equivalent stress, $\sigma_r$ is the reference stress related to lattice friction stress and Orowan effects [45], $\alpha = 0.4$ is a material constant, $G = E/(1 + 2\nu)$ is the shear modulus, $E = 196$ GPa is the elastic modulus, $\nu = 0.3$ is the Poisson ratio, and $b$ denotes the magnitude of Burgers vector. The initial dislocation densities (in absence of plastic deformation) of $2.5 \times 10^{14}$ m$^{-2}$ for B13 and that of $8.6 \times 10^{14}$ m$^{-2}$ for B15 were chosen based on the experimental data of a quench and tempered medium carbon steel [43], which corresponds with the $\sigma_r$ of 850 MPa and 610 MPa respectively. These values lie in the range $10^{14}$–$10^{15}$ m$^{-2}$ of tempered martensite [46] and give excellent predictions in the following sections.

The cohesive energy of GB without hydrogen $2\gamma_{gb}^0$ is taken as 3.12 J/m$^2$ and maximal hydrogen coverage of GB $\Gamma_{max}$ is $2.65 \times 10^{-5}$ mol/m$^2$ [47]. Following Olden et al. [28,29], the parameters for cohesive law were obtained by using one of the experimental data [2]. The cohesive strength and critical separation are adjusted till the resulting time to fracture equals to the selected experimental data. The elastic separation $\delta_0$ was assigned a value of $1 \times 10^{-7}$ mm based on the previous parametric study [28]. It has been shown that stress triaxiality has a marked impact on the interfacial decohesion which in turn influences the cohesive properties [48,49]. In this work, the stress triaxiality effect is decoupled from hydrogen degradation in the form of following equation [49]

$$\sigma_c(\delta_c, \eta, \theta_{T,gb}) = \sum(\delta_c, \eta)\cdot\Psi(\theta_{T,gb}) \tag{10}$$

where $\eta$ is the stress triaxiality, $\Psi(\theta_{T,gb})$ denotes hydrogen degradation function and $\sum(\delta_c, \eta)$ corresponds to the cohesive strength without hydrogen influence, i.e. $\sigma_c(0)$. Then, the variation of cohesive parameters due to different stress triaxiality are obtained by fitting the experimental data of different notch radius. The obtained cohesive properties of B13 and B15 without hydrogen influence are summarized in Table 2. It is clearly that the cohesive parameters strongly depend on stress triaxiality, i.e. the cohesive strength increases with the increase of notch radius while critical separation decreases, which is in accordance with the trends in literature [49,50].

**Table 1**
Material properties related to hydrogen diffusion.

| Parameters | Value | Reference |
|---|---|---|
| Partial molar volume of hydrogen $V_H$ | $2.0 \times 10^{-6}$ (m$^3$/mol) | [41] |
| Lattice site density $N_L$ | $8.46 \times 10^{28}$ (sites/m$^3$) | [12] |
| Lattice parameter $a$ | $2.8865 \times 10^{-10}$ (m) | [12] |
| Magnitude of the Burger's vector $b$ | $2.48 \times 10^{-10}$ (m) | [43] |
| Dislocation trap density $N_{T,d}$ | $\sqrt{2}\rho_d/a$ | [43] |
| Dislocation binding energy $\Delta g_{T,d}^0$ | 20.2 (kJ/mol) | [41,51–53] |
| Grain boundary density $N_{T,gb}$ | $10^{23}$ (sites/m$^3$) | [12,42] |
| Grain boundary binding energy $\Delta g_{T,gb}^0$ | 27.0 (kJ/mol) | [21,42,54] |
| Free surface binding energy $\Delta g_{T,FS}^0$ | 95.5 (kJ/mol) | [12,41] |

## Results and discussion

Fig. 3 illustrates the effects of applied load level, notch radius and holding time on the distributions of stress, plastic strain and hydrogen concentration near the notch root. As shown in Fig. 3(a), the stress peak becomes higher with increasing applied load level or decreasing notch radius, while its location moves away from the notch root when notch radius or applied load level increases. This is consistent with the stress concentration effect and the expansion of plastic zone. Since the hydrogen concentration is dominated by the stress, the similarity between the distributions of the stress and the hydrogen concentration is observed, Fig. 3(b, c). The distribution of hydrogen concentration at GB

**Table 2**
Summary of the cohesive parameters without hydrogen influence.

| | $\rho$ (mm) | $\sigma_c$ (0) (MPa) | $\delta_c$ ($\times 10^{-4}$ mm) |
|---|---|---|---|
| B13 | 0.10 | 3772 | 5.54 |
| B15 | 0.10 | 3315 | 4.03 |
| | 0.80 | 2636 | 5.07 |

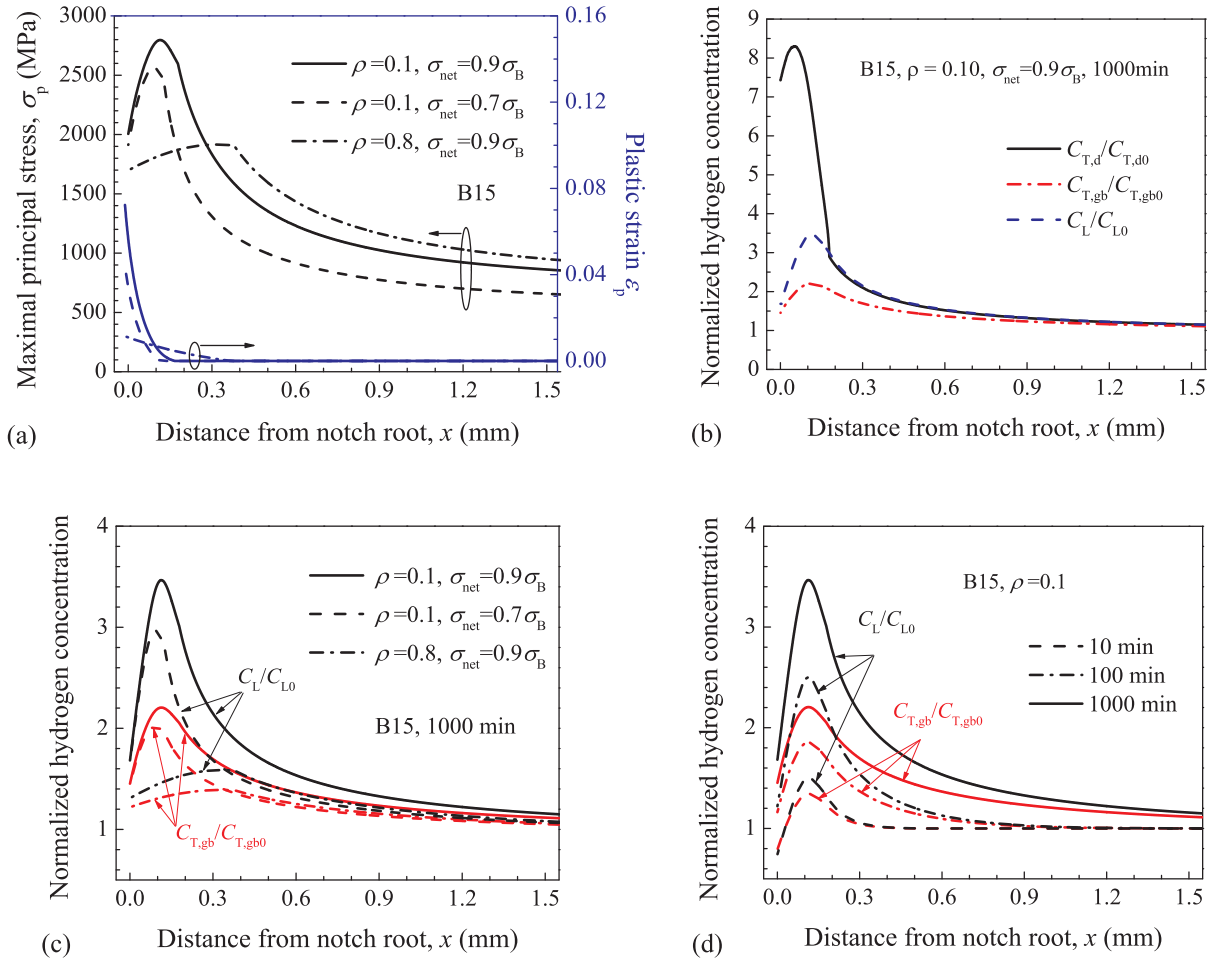


**Fig. 3.** Effects of applied load level, notch radius and holding time on distribution of stress, plastic strain and hydrogen concentration near notch root: (a) Stress and plastic strain distribution at various notch radius and applied load level for B15; (b) Distributions of normalized hydrogen concentration at NILS, dislocations and GB under applied load $\sigma_{app} = 0.9\sigma_B$ for B15 with notch radius $\rho = 0.1$ mm; (c) Distributions of normalized hydrogen concentration at NILS and GB at various notch radii and applied load levels; (d) Evolution of hydrogen distribution with increasing holding time. $C_{L0}$, $C_{T,d0}$ and $C_{T,gb0}$ are the initial values of the hydrogen concentration at NILS $C_L$, at dislocation trap sites $C_{T,d}$ and GB trap sites $C_{T,gb}$, respectively.

follows that of the NILS hydrogen, Fig. 3(b, c), due to the equilibrium assumption between hydrogen trapped at GB and hydrogen in NILS, i.e. Eq. (1). The peak hydrogen concentration at GB is in the vicinity of peak maximal principal stress site, as where stress-driven accumulation of NILS hydrogen also presents, Fig. 3(b). By contrast, the peak hydrogen concentration at dislocations is closer to notch root than the peak NILS hydrogen concentration and its normalized value is larger compared with the normalized NILS concentration and normalized concentration at GB, Fig. 3(b), because of the remarkable increase of dislocation densities near the notch root due to plastic deformation. The accumulation of hydrogen at NILS and GB is enhanced due to the enhanced stress concentration by increasing applied load level or decreasing notch radius as shown in Fig. 3(a). With increasing holding time, hydrogen concentration increases until reaching the steady state, Fig. 3(d).

Fig. 4(a) shows the calculated time to fracture as a function of the initial total diffusible hydrogen concentration $C_D$ along with the experimental data from [2] when applied load $\sigma_{app} = 0.9\sigma_B$. Good agreement is observed between the simulation and experimental results, indicating good capability of the present two-steps sequentially coupled diffusion-CZM approach. With increasing initial diffusible hydrogen content, the time to delayed fracture decreases quickly. But the delayed fracture would not take place when the initial total diffusible hydrogen concentration is lower enough (for example, when $C_D$ is lower than 0.05 wppm for the B15 with notch radius $\rho = 0.1$ at $\sigma_{app} = 0.9\sigma_B$, HIDF will not occur). To further reveal the meaning of this result, Fig. 4(b) displays the relationship between the initial NILS hydrogen concentration and peak hydrogen concentration at GB $C_{T,gb,p}$ at the failure of first cohesive element. The failure of the first cohesive element indicates crack initiation, thus the peak hydrogen concentration accumulated at GB at the failure of the first cohesive element is the critical GB hydrogen concentration for the local IG cracking. It is shown that the peak hydrogen concentration at GB at cracking initiation does not depend on the initial hydrogen content, indicating that the delayed fracture would not occur at a given applied load level when the initial hydrogen concentration is too low to gather to the critical values even the holding time is very long. This is consistent with the delayed fracture tests of high-strength steels [2,55,56]. The results indicate that the critical GB hydrogen concentration is independent on the initial uniform hydrogen concentration, also in line with [2,55,56].

Fig. 5(a) shows the effects of applied load level and notch radius on the time to failure for B15 with initial NILS hydrogen concentration $C_{L0} = 0.10$ wppm. At a given initial NILS concentration, the time to fracture increases with decreasing applied load level. When the applied load level is small enough, delayed fracture cannot occur, Fig. 5(a), due to unsatisfied stress condition needed for hydrogen accumulation and crack initiation. Thus, applied load level has a threshold value for a given initial hydrogen concentration and notch radius. As the applied load level is large enough, fracture happens just loaded, as shown in Fig. 5(a). These results are consistent with the experimental trend in

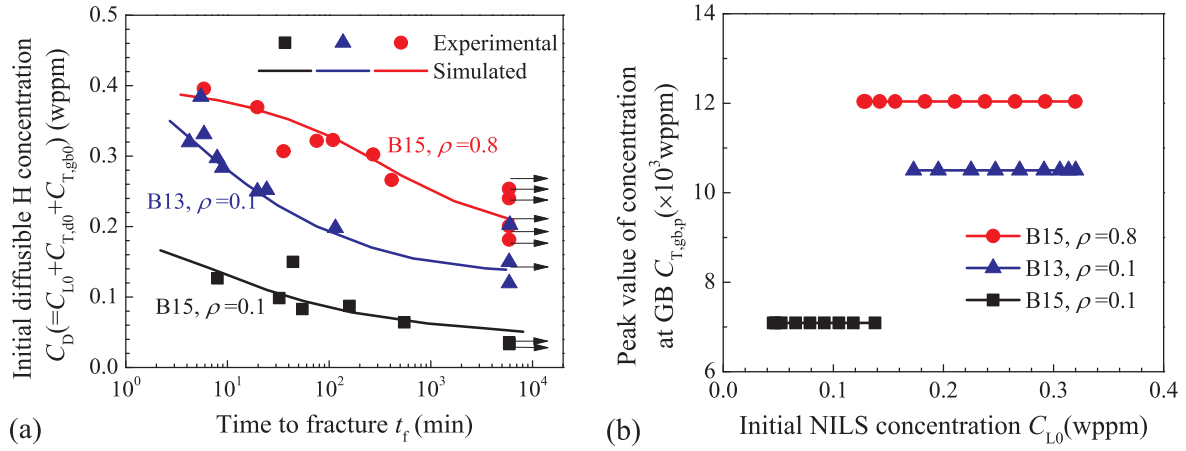


**Fig. 4.** Comparison between simulated and experimental data of time to failure in [2] for B13 and B15 steel as a function of initial diffusible hydrogen concentration (a); Peak hydrogen concentration at GB at failure as a function of initial NILS hydrogen concentration (b). The data points marked with an arrow in the figure indicate no fracture was observed.

literature [2,55]. With increasing notch radius, time to delayed fracture increases due to less concentrated stress.

Fig. 5(b) plots the relationship between the peak value of maximal principal stress and peak hydrogen concentrations at GB at failure i.e. the critical GB hydrogen concentration for IG cracking initiation. It can be seen that critical GB hydrogen concentration linearly decreases with increasing peak value of maximal principal stress, indicating that critical hydrogen concentration depends strongly on local stress level, despite that it is independent on the initial hydrogen concentration. A higher peak value of maximal principal stress can not only concentrate hydrogen more rapidly but also require a lower critical hydrogen concentration to initiate cracking. However, for different notch radii under different remote applied load levels, even if the resulting local maximal principle stresses are identical, the critical hydrogen concentrations are distinctly different (it is surprising that at the same local maximal principle stress, $\rho = 0.1$ has a higher rather than lower critical hydrogen concentration than $\rho = 0.8$), indicating the important influence of notch radius i.e. stress triaxiality on the hydrogen-induced fracture. Table 2 has shown that lower notch radius has a higher critical cohesive strength for crack initiation due to lower stress triaxiality, thus lower notch radius has a higher rather than lower critical hydrogen concentration. Fig. 5(b) also depicts the critical GB hydrogen concentration as a function of the normalized peak maximal principal stress (dividing the peak maximal principal stress by the critical cohesive strength in absence of hydrogen). By normalizing the peak maximal principal stress, it is shown that the critical hydrogen concentration becomes the only function of the normalized peak maximal principal stress. Thus, it seems that the critical hydrogen concentration can be related quantificationally to the normalized peak maximal principal stress. It can be concluded that the critical hydrogen concentration is an inverse function of the normalized peak maximal principal stress, although it is independent on the initial uniform hydrogen concentration.

The present two-steps sequentially coupled hydrogen diffusion-CZM approach has successfully reproduced the experimental data of constant load tests in [2]. The effects of both dislocation trap sites and GB trap sites are considered in the diffusion analysis. The relationship between the hydrogen coverage of GB and cohesive strength is quantificationally described based on the theory of thermodynamic decohesion. Two important aspects characterizing the delayed fracture of high-strength steels, i.e. the critical hydrogen concentration at a given load level and the threshold stress at a given initial hydrogen content, is captured. The critical hydrogen concentration is independent on the initial hydrogen concentration but linearly decreases with increasing normalized peak maximal principal stress. In fact, it is also found that the calculated crack initiation site is close to the peak maximal principal stress site, which located in the intergranular fracture region, in accordance with

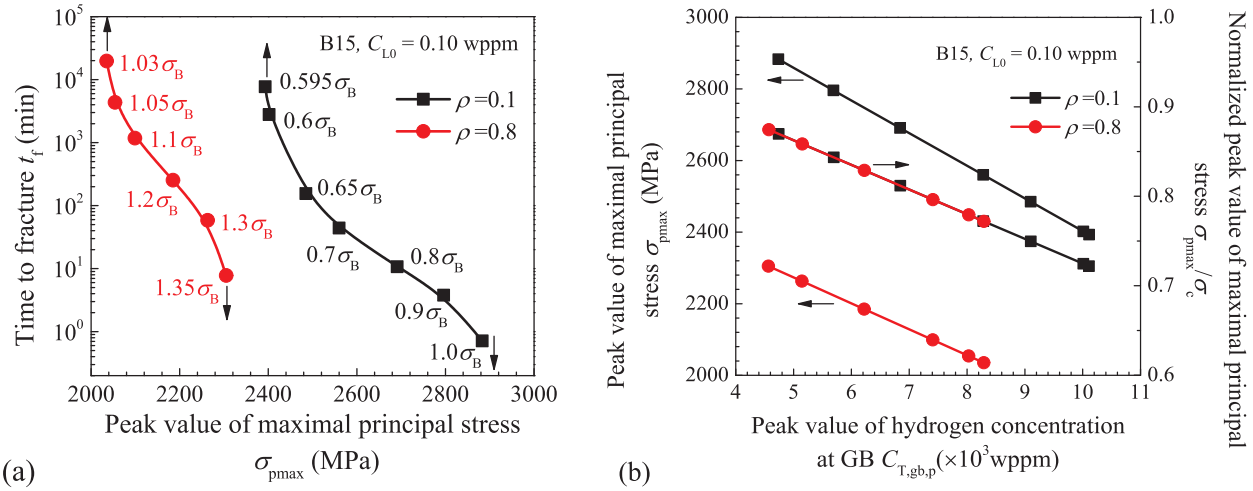


**Fig. 5.** Effects of applied load level and notch radius on time to failure for B15 with initial NILS hydrogen concentration $C_{L0} = 0.10$ wppm (a); Peak value of maximal principal stress as a function of peak hydrogen concentrations at GB at failure (b). The texts marked near the data points is the value of applied load $\sigma_{app}$.

the experimental observations [3]. It should be noted that the present study uses the crack initiation time as the time to fracture, which is reasonable since the crack growth quickly after initiation due to brittle intergranular fracture. However, the present study does not explicitly include the effect of stress triaxiality on the cohesive parameters akin to the approach in [50]. This aspect will be investigated in our future research.

## Summary

The present study has developed a two-steps sequential coupled diffusion-CZM approach for predicting HIDF of high-strength steels. The approach takes account of the influence of multiple hydrogen trap sites (dislocation trap sites and GB trap sites) on hydrogen transport and fracture. Damage effect of hydrogen on GB separations was implemented into TSL based on the classic thermodynamic decohesion theory. The numerical results were compared with the experimentally measured time to failure for an AISI 4135 steel. Good agreement is observed between the simulation and experimental results in terms of time to failure, implying good prediction capability of the coupled CZM approach in HIDF of high-strength steels. The results confirm that hydrogen concentration trapped at GB can be related to the hydrogen-induced intergranular fracture of high strength low-alloy steels. The critical hydrogen concentration for crack initiation is independent of initial hydrogen concentration but depends strongly on local stress level and stress triaxiality. The critical hydrogen concentration linearly decreases with increasing normalized peak maximal principal stress.

## Acknowledgements

The authors would like to acknowledge the financial support of the National Natural Science Foundation of China (No. 51505477) and the Fundamental Research Funds for the Central Universities of China (2015QNA20).

## References

[1] Gangloff RP. Hydrogen assisted cracking of high strength alloys. Compr Struct Integr 2003;6:31–101.
[2] Wang M, Akiyama E, Tsuzaki K. Determination of the critical hydrogen concentration for delayed fracture of high strength steel by constant load test and numerical calculation. Corros Sci 2006;48:2189–202.
[3] Wang M, Akiyama E, Tsuzaki K. Effect of hydrogen on the fracture behavior of high strength steel during slow strain rate test. Corros Sci 2007;49:4081–97.
[4] Serebrinsky S, Carter EA, Ortiz M. A quantum-mechanically informed continuum model of hydrogen embrittlement. J Mech Phys Solids 2004;52:2403–30.
[5] Troiano AR. The role of hydrogen and other interstitials in the mechanical behavior of metals. Trans ASM 1960;52:54–80.
[6] Oriani RA. Whitney award lecture—1987: Hydrogen—The versatile embrittler. Corrosion 1987;43:390–7.
[7] Gerberich WW, Marsh PG, Hoehn JW. Hydrogen induced cracking mechanisms—are there critical experiments? In: Thompson AW, Moody NR, editors. Hydrogen effects in materials. Warrendale, PA: TMS; 1996. p. 539–51.
[8] Robertson IM. The effect of hydrogen on dislocation dynamics. Eng Fract Mech 1999;64:649–73.
[9] Nagao A, Dadfarnia M, Sofronis P, Robertson IM. Hydrogen embrittlement: mechanisms. In: Totten GE, Colás R, editors. Encyclopedia of iron, steel, and their alloys. London: Taylor & Francis; 2016. p. 1768–84.
[10] Gerberich WW, Stauffer DD, Sofronis P. HELP and HEDE. Effects of hydrogen on materials—proceedings of the 2008 international hydrogen conference. ASM International; 2008. p. 38–45.
[11] San Marchi C, Somerday BP, Tang X, Schiroky GH. Effects of alloy composition and strain hardening on tensile fracture of hydrogen-precharged type 316 stainless steels. Int J Hydrogen Energy 2008;33:889–904.
[12] Novak P, Yuan R, Somerday BP, Sofronis P, Ritchie RO. A statistical, physical-based, micro-mechanical model of hydrogen induced intergranular fracture in steel. J Mech Phys Solids 2010;58:105–23.
[13] Djukic MB, Sijacki Zeravcic V, Bakic G, Sedmak A, Rajicic B. Hydrogen embrittlement of low carbon structural steel. Procedia Mater Sci 2014;3:1167–72.
[14] Djukic MB, Sijacki Zeravcic V, Bakic GM, Sedmak A, Rajicic B. Hydrogen damage of steels: A case study and hydrogen embrittlement model. Eng Fail Ana 2015;58:485–98.
[15] Djukic MB, Bakic GM, Sijacki Zeravcic V, Sedmak A, Rajicic B. Hydrogen embrittlement of industrial components: prediction, prevention and models. Corrosion 2016;72:943–61.
[16] Djukic MB, Bakic GM, Sijacki Zeravcic V, Rajicic B, Sedmak A, Mitrovic R, et al. Towards a unified and practical industrial model for prediction of hydrogen embrittlement and damage in steels. Procedia Struct Integrity 2016;2:604–11.
[17] Nagao A, Martin ML, Dadfarnia M, Sofronis P, Robertson IM. The effect of nano-sized (Ti, Mo)C precipitates on hydrogen embrittlement of tempered lath martensitic steel. Acta Mater 2014;74:244–54.
[18] Nagao A, Smith CD, Dadfarnia M, Sofronis P, Robertson IM. The role of hydrogen in hydrogen embrittlement fracture of lath martensitic steel. Acta Mater 2012;60:5182–9.
[19] Nagao A, Smith CD, Dadfarnia M, Sofronis P, Robertson IM. Interpretation of hydrogen-induced fracture surface morphologies for lath martensitic steel. Procedia Mater Sci 2014;3:1700–5.
[20] Nagao A, Dadfarnia M, Somerday BP, Sofronis P, Ritchie RO. Hydrogen-enhanced-plasticity mediated decohesion for hydrogen-induced intergranular and "quasi-cleavage" fracture of lath martensitic steels. J Mech Phys Solids 2018;112:403–30.
[21] Gerberich WW, Livne T, Chen XF, Kaczorowski M. Crack growth from internal hydrogen—temperature and microstructure effects in 4340 steel. Metall Trans A 1988;19:1319–34.
[22] Wang R. Effects of hydrogen on the fracture toughness of a X70 pipeline steel. Corros Sci 2009;51:2803–10.
[23] Lunarska E, Ososkov Y, Jagodzinsky Y. Correlation between critical hydrogen concentration and hydrogen damage of pipeline steel. Int J Hydrogen Energy 1997;22:279–84.
[24] Capelle J, Gilgert J, Dmytrakh I, Pluvinage G. Sensitivity of pipelines with steel API X52 to hydrogen embrittlement. Int J Hydrogen Energy 2008;33:7630–41.
[25] Singh DK, Maiti SK, Bhandakkar TK, Raman RKS. Efficient approach for cohesive zone based three-dimensional analysis of hydrogen-assisted cracking of a circumferentially notched round tensile specimen. Int J Hydrogen Energy 2017;42:15943–55.
[26] Liang Y, Sofronis P. Toward a phenomenological description of hydrogen-induced decohesion at particle/matrix interfaces. J Mech Phys Solids 2003;51:1509–31.
[27] Jemblie L, Olden V, Akselsen OM. A coupled diffusion and cohesive zone modelling approach for numerically assessing hydrogen embrittlement of steel structures. Int J Hydrogen Energy. 2017;42:11980–95.
[28] Olden V, Thaulow C, Johnsen R, Østby E, Berstad T. Application of hydrogen influenced cohesive laws in the prediction of hydrogen induced stress cracking in 25%Cr duplex stainless steel. Eng Fract Mech 2008;75:2333–51.
[29] Olden V, Thaulow C, Johnsen R, Østby E, Berstad T. Influence of hydrogen from cathodic protection on the fracture susceptibility of 25%Cr duplex stainless steel – Constant load SENT testing and FE-modelling using hydrogen influenced cohesive zone elements. Eng Fract Mech 2009;76:827–44.
[30] Pressouyre GM. Trap theory of hydrogen embrittlement. Acta Metall 1980;28:895–911.
[31] Oriani RA. The diffusion and trapping of hydrogen in steel. Acta Metall 1970;18:147–57.
[32] Hirth JP, Rice JR. On the thermodynamics of adsorption at interfaces as it influences decohesion. Metall Trans A 1980;11:1501–11.
[33] Rice JR, Wang JS. Embrittlement of interfaces by solute segregation. Mater Sci Eng A 1989;107:23–40.
[34] Hillerborg A, Modéer M, Petersson PE. Analysis of crack formation and crack growth in concrete by means of fracture mechanics and finite elements. Cem Concr Res 1976;6:773–81.
[35] Jiang W, Chen W, Woo W, Tu ST, Em V. Effects of low-temperature transformation and transformation-induced plasticity on weld residual stresses: numerical study and neutron diffraction measurement. Mater Design 2018;147:65–79.
[36] Jiang W, Zhang Y, Woo W. Using heat sink technology to decrease residual stress in 316L stainless steel welding joint: finite element simulation. Int J Press Vess Pip 2012;92:56–62.
[37] Xie X, Jiang W, Luo Y, Xu S, Tu ST. A model to predict the relaxation of weld residual stress by cyclic load: experimental and finite element modeling. Int J Fatigue 2017;95:293–301.
[38] Díaz A, Alegre JM, Cuesta II. Coupled hydrogen diffusion simulation using a heat transfer analogy. Int J Mech Sci 2016;115–116:360–9.
[39] Barrera O, Tarleton E, Tang HW, Cocks ACF. Modelling the coupling between hydrogen diffusion and the mechanical behaviour of metals. Comput Mater Sci 2016;122:219–28.
[40] Yu H, Olsen JS, Olden V, Alvaro A, He J, Zhang Z. Viscous regularization for cohesive zone modeling under constant displacement: an application to hydrogen embrittlement simulation. Eng Fract Mech 2016;166:23–42.
[41] Hirth JP. Effects of hydrogen on the properties of iron and steel. Metall Trans A 1980;11:861–90.
[42] Pressouyre GM. A classification of hydrogen traps in steel. Metall Trans A 1979;10:1571–3.
[43] Dadfarnia M, Sofronis P, Neeraj T. Hydrogen interaction with multiple traps: can it be used to mitigate embrittlement? Int J Hydrogen Energy 2011;36:10141–8.
[44] Kocks U, Mecking H. Physics and phenomenology of strain hardening: the FCC case. Prog Mater Sci 2003;48:171–273.
[45] Malik L, Lund JA. A study of strengthening mechanisms in tempered martensite from a medium carbon steel. Metall Trans 1972;3:1403–6.
[46] Iza-Mendia A, Gutiérrez I. Generalization of the existing relations between microstructure and yield stress from ferrite-pearlite to high strength steels. Mater Sci Eng A 2013;561:40–51.
[47] Wang JS, Vehoff H. The effect of the mobility of segregated atoms on interfacial embrittlement. Scr Metall Mater 1991;25:1339–44.
[48] Needleman A. A continuum model for void nucleation by inclusion debonding. J

Appl Mech 1987;54:525–31.
[49] Yu H, Olsen JS, Alvaro A, Olden V, He J, Zhang Z. A uniform hydrogen degradation law for high strength steels. Eng Fract Mech 2016;157:56–71.
[50] Anvari M, Scheider I, Thaulow C. Simulation of dynamic ductile crack growth using strain-rate and triaxiality-dependent cohesive elements. Eng Fract Mech 2006;73:2210–28.
[51] Choo WY, Lee JY. Thermal analysis of trapped hydrogen in pure iron. Metall Trans A 1982;13:135–40.
[52] Choo WY, Lee JY. Effect of cold working on the hydrogen trapping phenomena in pure iron. Metall Trans A 1983;14:1299–305.
[53] Takita K, Sakamoto K. Low temperature internal friction peak and hydrogen cold-work peak in deformed α-iron. Scripta Metall 1976;10:399–403.
[54] Bernstein IM. The effect of hydrogen on the deformation of iron. Scripta Metall 1974;8:343–9.
[55] Johnson HH, Morlet JG, Troiano AR. Hydrogen, crack initiation, and delayed failure in steels. Trans Metall Soc AIME 1958;212:528–36.
[56] Kimura Y, Sakai Y, Hara T, Belyakov A, Tsuzaki K. Hydrogen induced delayed fracture of ultrafine grained 0.6% O steel with dispersed oxide particles. Scripta Mater 2003;49:1111–6.